Mantled and exhumed terrains in Terra Meridiani, Mars

R. E. Arvidson, F. P. Seelos IV, K. S. Deal, W. C. Koeppen, N. O. Snider,
J. M. Kieniewicz, and B. M. Hynek
McDonnell Center for the Space Sciences, Department of Earth and Planetary Sciences, Washington University, St. Louis, Missouri, USA

M. T. Mellon
Laboratory for Atmospheric and Space Physics, University of Colorado, Boulder, Colorado, USA

J. B. Garvin
NASA Goddard Space Flight Center, Greenbelt, Maryland, USA

Received 9 December 2002; revised 22 December 2002; accepted 22 December 2002; published 18 October 2003.

[1] Hematite-bearing deposits in the Terra Meridiani region of Mars constitute the top stratum of a partially eroded layered complex that covers dissected Noachian-aged cratered terrain. The hematite unit consists of dark plains and dunes covering a bright substrate. This substrate is fully exposed beyond the borders of the hematite-bearing deposit and consists of polygonal ground separated by ridges or valleys, together with layered deposits that have been eroded into a variety of landforms. The complex is partially covered by a regional-scale aeolian mantle that thickens toward the north. The hematite-bearing stratum exhibits low albedoes, pulse widths, and intermediate thermal inertias, whereas the underlying unit exhibits high values of these parameters. Both units have spectral emissivity signatures similar to those for the low albedo cratered terrain to the south, with the addition of hematite for the top stratum. The complex is interpreted to consist of extensive plains-forming lava flows and tephra deposits emplaced during an extensional regime and at least partially buried by an aeolian mantle. Aeolian stripping of the mantle exposed much of the complex and differentially eroded the deposits to produce the landforms existent today. Exploration of the hematite-bearing deposits by the 2003 Mars Exploration Rover, ''Opportunity,'' will allow testing of the hypotheses presented since this stratum has been locally reworked into dunes that only partially cover the underlying brighter portion of the complex. In particular, the rover-based measurements will allow us to test the extent to which the unusual remote-sensing properties of the units indicate aqueous alteration. *INDEX TERMS:* 6225 Planetology: Solar System Objects: Mars; 5470 Planetology: Solid Surface Planets: Surface materials and properties; 5464 Planetology: Solid Surface Planets: Remote sensing; 5415 Planetology: Solid Surface Planets: Erosion and weathering; *KEYWORDS:* Mars, Mars Exploration Rover Mission, Terra Meridiani

Citation: Arvidson, R. E., F. P. Seelos IV, K. S. Deal, W. C. Koeppen, N. O. Snider, J. M. Kieniewicz, B. M. Hynek, M. T. Mellon, and J. B. Garvin, Mantled and exhumed terrains in Terra Meridiani, Mars, *J. Geophys. Res.*, *108*(E12), 8073, doi:10.1029/2002JE001982, 2003.

1. Introduction

[2] The purpose of this paper is to summarize analyses of Mars Global Surveyor MOC [*Malin and Edgett*, 2001], MOLA [*Smith et al.*, 2001], and TES [*Christensen et al.*, 2001a] observations to identify, characterize, map, and understand the origin and evolution of the hematite-bearing deposits [*Christensen et al.*, 2000a, 2001a] and associated units in the Terra Meridiani region of Mars (Figures 1, 2a, and 2b). The approach is to use MOC wide-angle and narrow-angle images (WA and NA, respectively), together with elevation estimates from MOLA data, to define and map units on the basis of morphology and superposition relationships. Surface properties of these units are then characterized using MOLA-based intrashot pulse widths [*Garvin et al.*, 1999] and TES-based albedoes, thermal inertias [*Mellon et al.*, 2001], and spectral emissivities [*Smith et al.*, 2000]. The data indicate that: (a) the hematite-bearing unit is the remnant of the top stratum of a widespread layered complex that was deposited onto dissected cratered terrain, (b) the complex was covered at least in the northern portions of Terra Meridiani by a widespread sedimentary mantle, (c) the entire region has been subjected to differential aeolian erosion that has stripped the mantle, exposing underlying materials that in turn have

0148-0227/03/2002JE001982$09.00

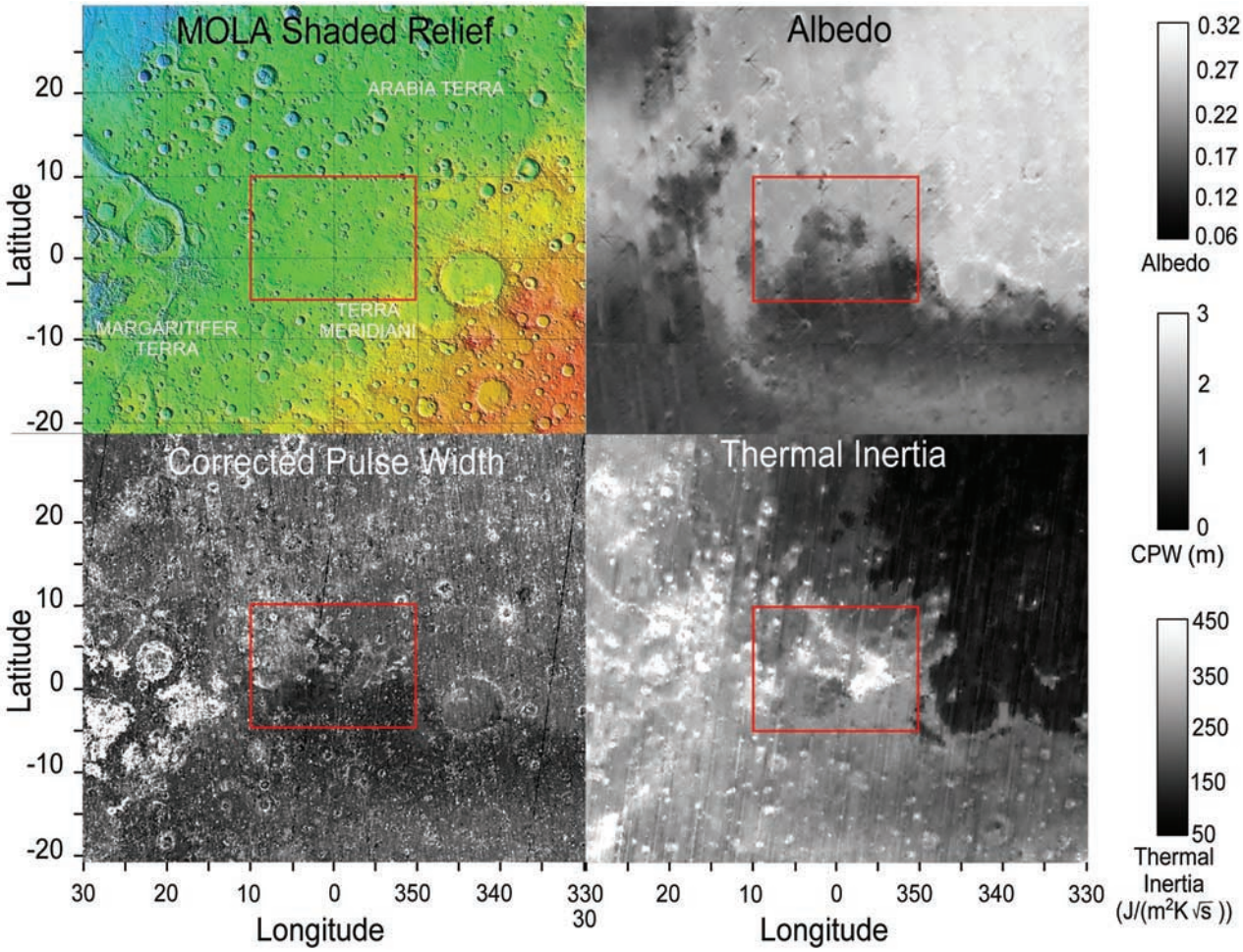

Figure 1. Series of frames showing the regional context and remote-sensing properties for the Terra Meridiani study area (boxed region). Color-coded shaded relief from MOLA data on upper left shows reds as high elevations (+3 km above MOLA-defined datum) and blues as low areas (−3 km relative to datum). TES-based albedo and thermal inertia estimates are shown on the upper and lower right, respectively. MOLA-based pulse widths (corrected for regional slopes) are shown on lower left.

been partially eroded by wind, and (d) the layered complex was emplaced as flows and tephra deposits, and the unusual albedo and spectral properties are consistent with alteration involving aqueous fluids, either during or after emplacement.

2. Definition of Geologic Units and Stratigraphy Based on Morphology, Topography, and Hematite Index

[3] This work builds on initial mapping of the Terra Meridiani study area (5 degrees south to 10 degrees north latitude and 20 degrees in longitude centered on the prime meridian) by *Hynek et al.* [2002]. It extends that mapping by incorporating all NA images within the study area acquired as part of the detailed survey of the planet [*Malin and Edgett*, 2001] and frames targeted on the MER landing sites located on the hematite-bearing deposits discovered by *Christensen et al.* [2000b, 2001b]. The study area boundaries were defined to include the hematite-bearing deposits and the borders of the underlying units within the layered units mapped by *Hynek et al.* [2002] (Figure 1).

[4] The first step in the work was the construction of a digital base map from 32 pixel/degree MOLA elevation data processed to remove regional tilts and thus to highlight local relief. The WA red mosaic compiled by *Caplinger and Malin* [2001] at 256 pixels/degree was co-registered to the MOLA map and the data sets merged by overlaying color-coded elevations onto the WA mosaic. Map units were defined from this product at a scale of 1:1,000,000, aided by examination of individual MOLA elevation profiles and NA frames located within the study area. NA frames were processed to Level 2 (i.e., in Universal Transverse Mercator format with units proportional to radiance on sensor) using the USGS Integrated Software for Imagers and Spectrometers (ISIS) software in order to place calibrated NA data in the merged WA and MOLA spatial framework. The MOLA, WA, and NA data were thus used in combination to identify and map the units on the basis of planimetric configuration, topography, brightness, and texture and to infer superposition and embayment relationships (Figures 2a and 2b). Further, the boundary of the hematite-bearing deposits was delineated using the hematite index threshold as defined by *Christensen et al.* [2001a] (Figures 2a and 2b).

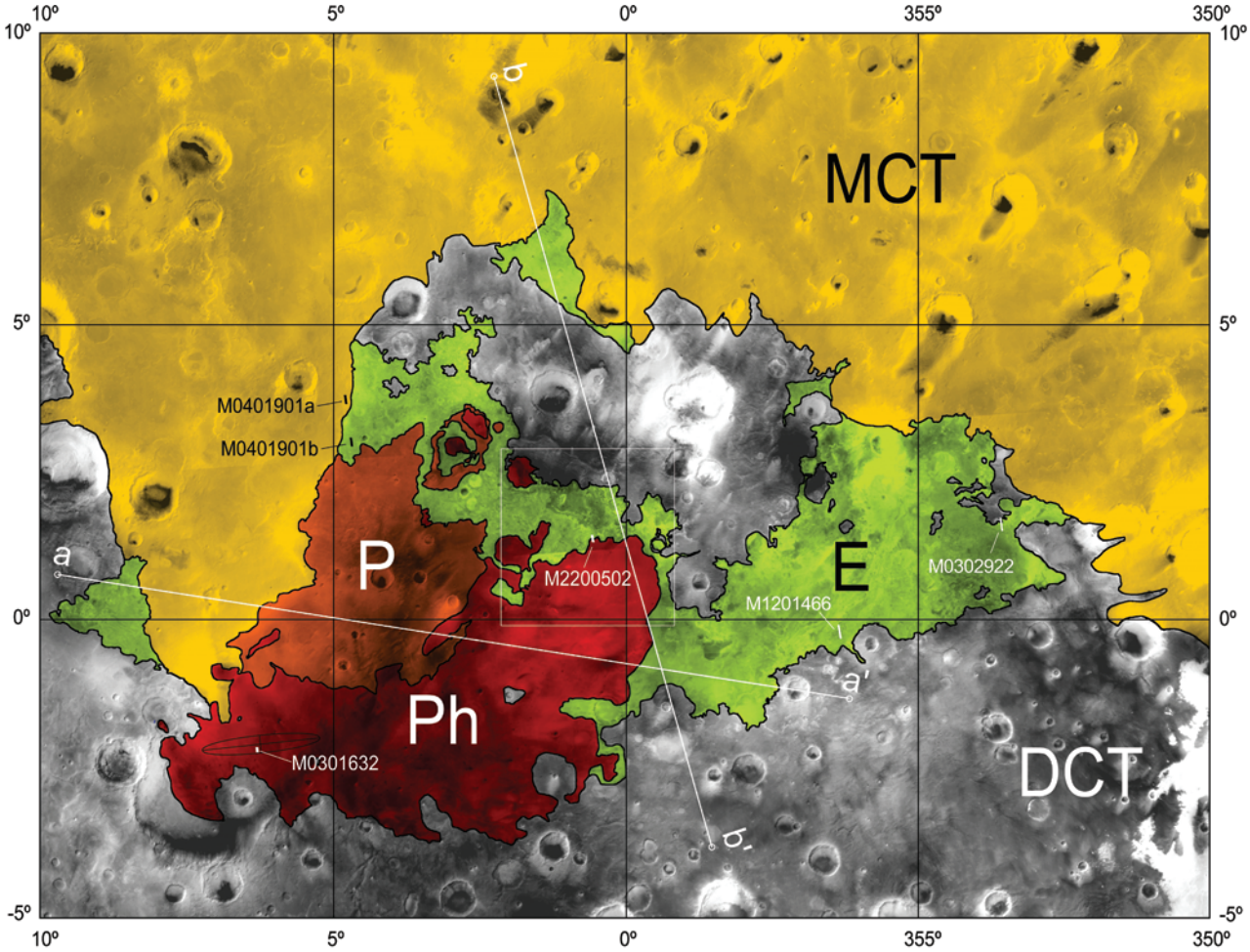

Figure 2a. Geologic map for the study area. Unit DCT corresponds to Noachian dissected cratered terrain and is the oldest unit exposed. Unit E is the etched unit that overlies the DCT unit and corresponds to a complex set of landforms, including polygonal ground, ridges, mesas, buttes, and features that appear to be yardangs. Unit Ph is a hematite bearing plains deposit that transitions to Unit P. P and Ph overlie E. MCT corresponds to mantled terrain, with other units exposed, but mantled by tens of meters of aeolian deposits. Also shown are locations of cross sections shown in Figure 2b, MOC NA footprints for images shown as figures in this paper, the rover landing error ellipse, and a white box that corresponds to the location covered by the MOLA map shown in Figure 6a.

[5] Regionally, the study area is within the Noachian-aged heavily cratered terrain in the northern part of Terra Meridiani (Figure 1). The lithosphere within the study area tilts downward to the northwest and has been postulated to have undergone flexure during the Noachian Epoch by the load associated with the formation of the Tharsis volcanic complex [*Phillips et al.*, 2001]. The presence of numerous channels and topographic outliers exposed on a regional scale suggests dissection of the Noachian cratered terrain by fluvial activity immediately after tilting, perhaps due to warm and wet conditions induced by extensive degassing associated with early Tharsis-related volcanism [*Hynek and Phillips*, 2001]. The layered complex was then disconformably emplaced over the dissected cratered terrain, most likely during late Noachian or early Hesperian time [*Hynek et al.*, 2002].

[6] The basal unit in the study area is the Noachian cratered terrain that has been extensively dissected by channel systems and is termed the dissected cratered terrain or Unit DCT (Figures 2a and 2b). The basal unit of the layered complex was termed the etched unit by *Hynek et al.* [2002] and we retain that nomenclature here as Unit E. On the basis of detailed analysis of WA and NA data, the morphology of Unit E is variable and includes extensive exposures of terrain characterized by: (a) relatively flat, dark polygonal blocks separated by bright, fractured ridges and occasionally by valleys (Figure 3); (b) interconnected ridges and stepped plateaus that demarcate underlying plains into polygonal patterns (Figure 4); and (c) landforms that consist of buttes, mesas, and what appear to be yardangs, often exposing layered deposits on cliff faces and slopes (Figures 5a and 5b). Analysis of superposition relationships shows that polygonal ground can be found both stratigraphically below and above the layered deposits, depending on the region under consideration.

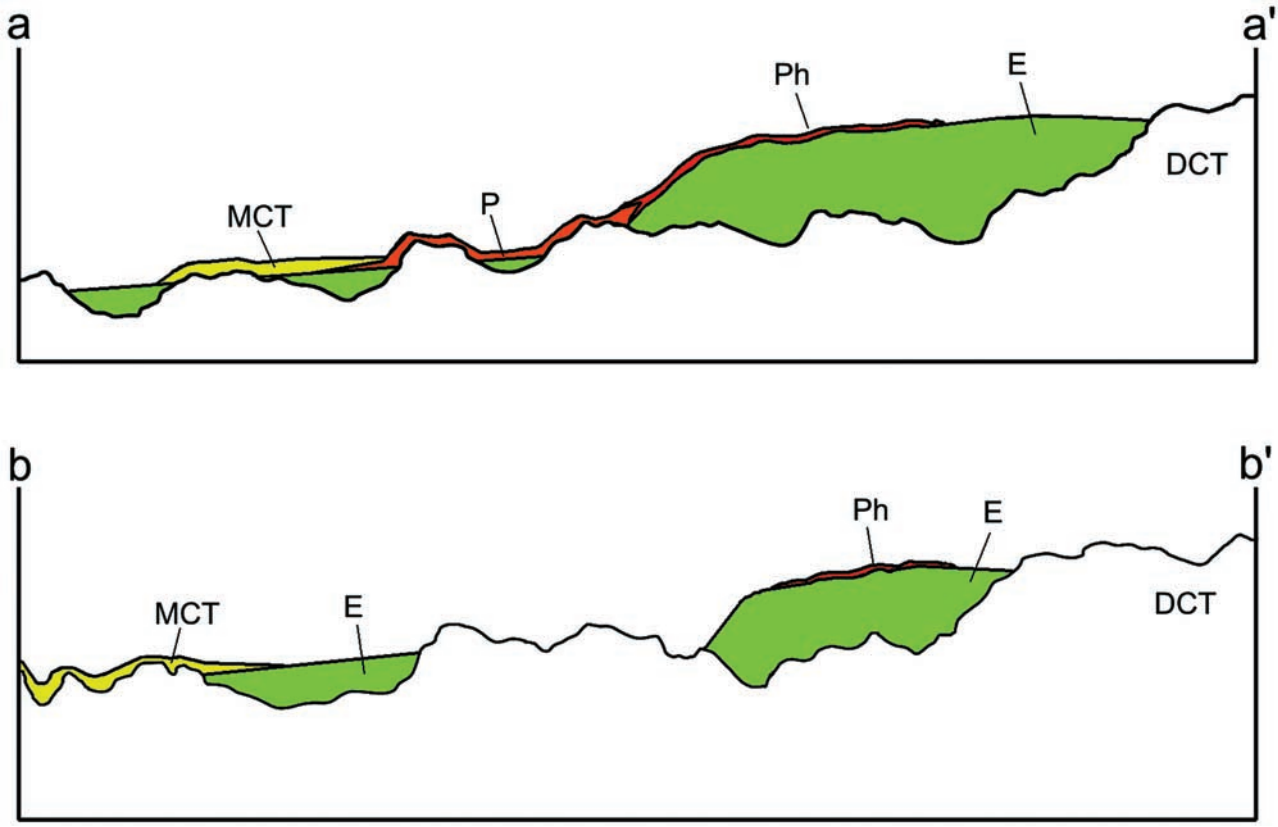

Figure 2b. Schematic cross sections through the study region derived from MOLA topography and shown with a 20:1 vertical exaggeration.

[7] The buttes, mesas, and yardang-like features evident in Unit E demonstrate that significant aeolian erosion has occurred, stripping up to several hundred meters from this deposit. For example, sections exposed on the northeastern boundary of Unit E show a transition from well-preserved polygonal ground within Unit E to partially eroded remnants of polygonal ground toward the edge of the deposits, to exposures of underlying layered deposits that have been scoured by wind at the contact with Unit DCT (Figures 5a and 5b). The eroded landforms, dunes, and streaks indicate that easterly winds were responsible for the scouring of the deposits.

[8] Detailed analyses of WA and NA images, MOLA gridded elevation data, and individual MOLA profiles registered to NA frames show that the hematite-bearing plains unit (Ph) is stratigraphically above the Unit E. NA data show that Unit Ph consists of smooth, dark plains that are locally reworked into dunes and that in many places only partially cover Unit E. This relationship is particularly well demonstrated at the northeastern boundary between Units Ph and E (Figures 6a and 6b). In that location the northern edge of Unit Ph corresponds to the edge of a rolling plateau. To the north of the plateau edge Unit E extends as a mappable unit for tens of kilometers, exposing several sections of layered deposits. Moving south from the Ph-E boundary it is clear that the interdune areas are exposures of Unit E (Figures 6a and 6b). This same pattern of dark deposits covering brighter materials is also evident within the hematite-bearing deposits located within the MER landing error ellipse (Figure 7). Finally, the northwestern edge of the Ph unit seems to transition to another plains-forming surface, herein termed Unit P (Figures 2a and 2b). Stratigraphic relationships are hard to define in detail because of a paucity of NA coverage. On the basis of available evidence we believe that Unit P is a lateral facies variation and that both deposits overlie Unit E.

[9] Units DCT, E, P, and Ph are covered by a mantle in the northern portion of the study area that has been partially stripped by aeolian processes to expose underlying materials. The mantled unit largely occurs on Noachian cratered terrain and is mapped as mantled cratered terrain unit or Unit MCT (Figures 2a and 2b). Examination of WA and NA images covering the boundary between the Units E and MCT shows that the characteristics associated with Unit E landforms become muted and even disappear beneath the mantle that defines Unit MCT (e.g., Figures 4 and 8). South of the contact, ridges and conical hills associated with Unit E are sharply defined, with flanks and walls that have distinct intersections with the surrounding terrain (Figure 4). Just to the north of the boundary only the ridges and tall conical hills associated with the E unit are exposed (Figure 8). The thickness of the mantle can be inferred by examination of individual MOLA elevation profiles and comparison of the exposed and mantled portions of the E Unit. For example, in MOC NA Frame M0401901 the ridges are approximately 20–30 m above the plains to the south of the boundary whereas to the north of the boundary only the tops of the

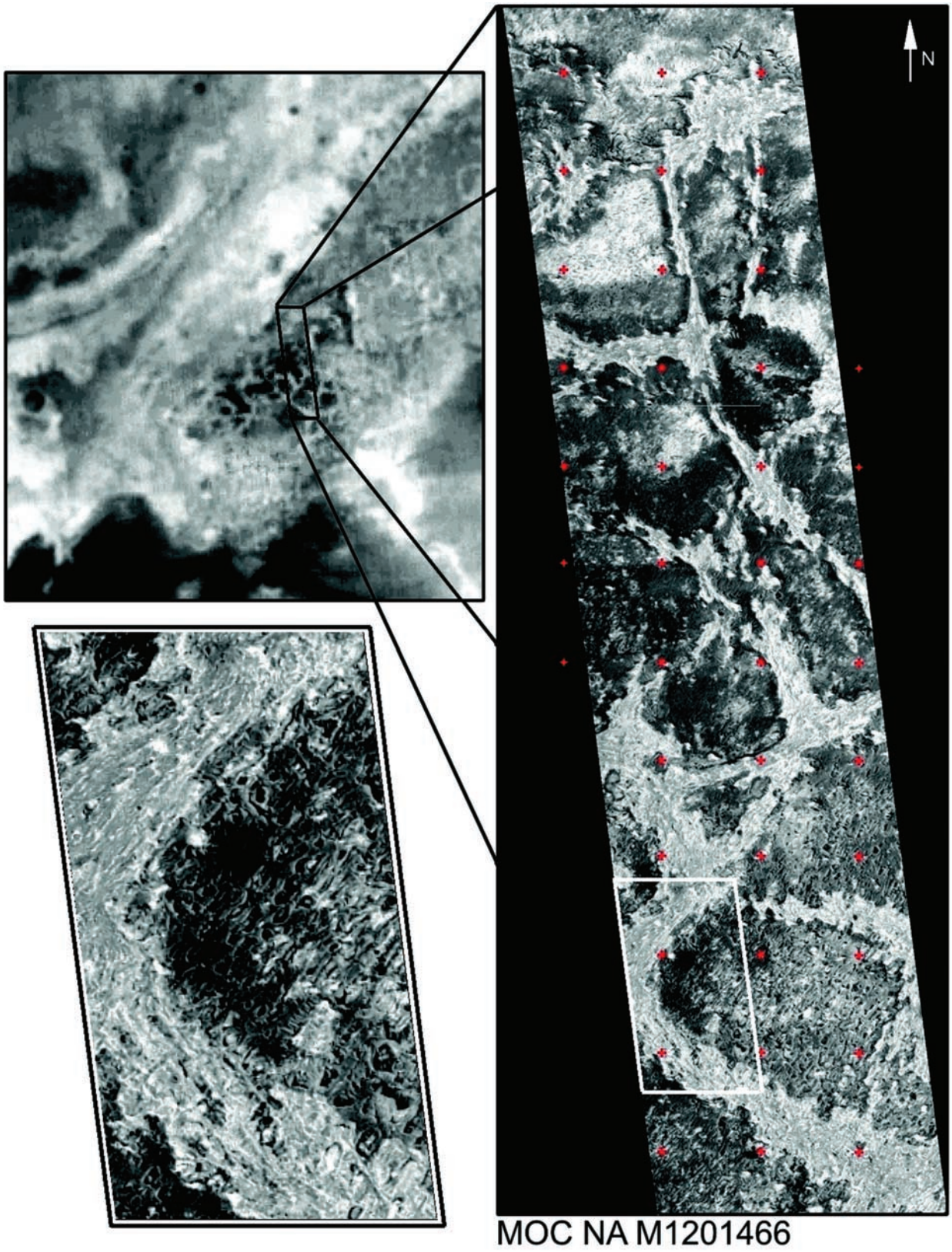

Figure 3. MOC WA frame M12-01467 and NA frame M12-01466 showing the morphology of the polygonal ground associated with Unit E. Bright ridges separating the polygons range from 10 to 40 m in elevation above the polygons, based on MOLA Orbit 14193 data. The polygonal terrain disappears beneath brighter terrain to both the north and south of the region shown in the NA data. UTM Projection with 1 minute spacing (approximately 1 km) between red crosses in this and subsequent figures showing NA data.

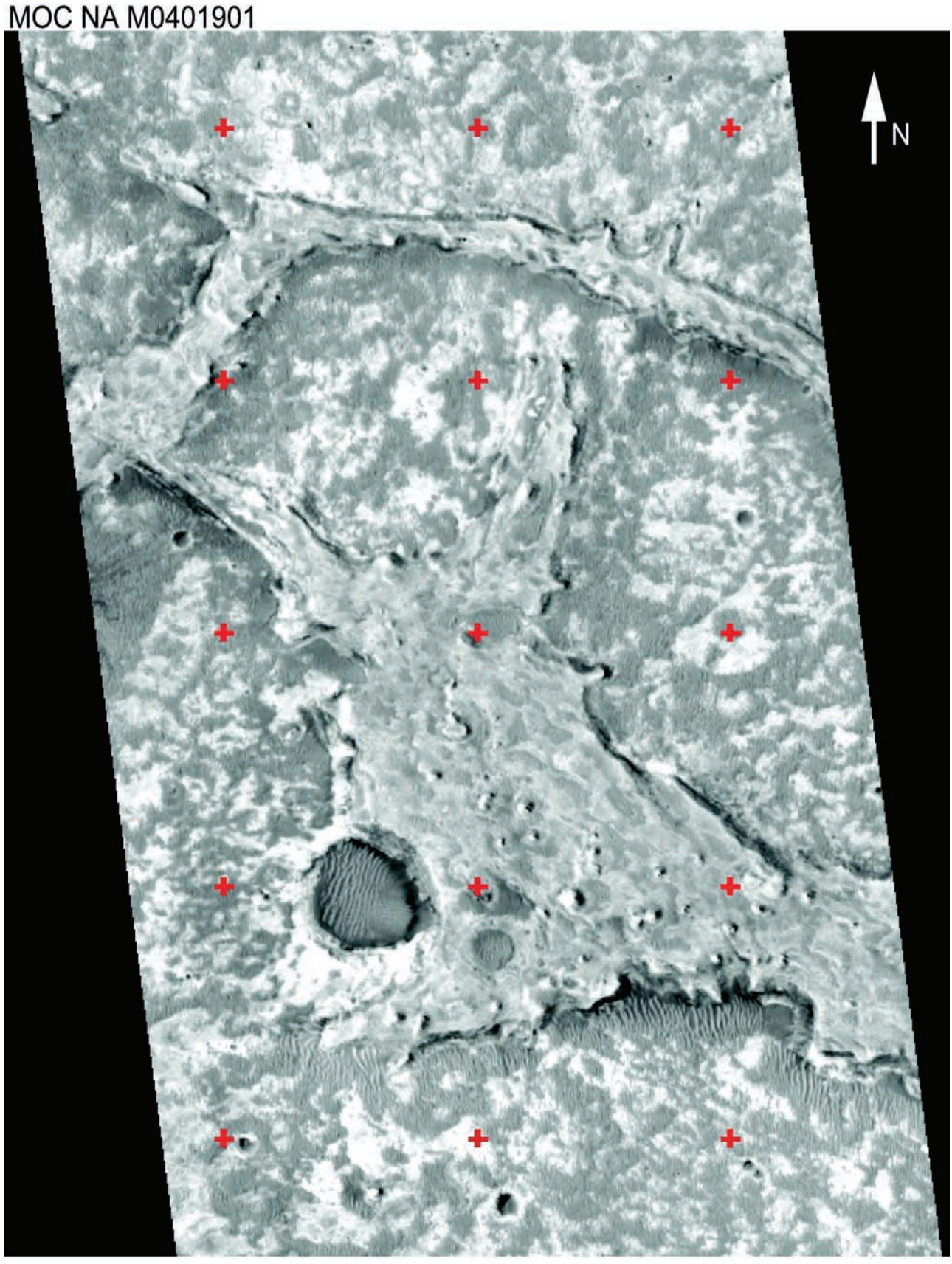

Figure 4. Portion of MOC NA frame M04-01901 showing Unit E with interconnected ridges and plateaus. The large plateau in the middle of the frame stands 21 m above the surrounding plains, based on examination of data from MOLA Orbit 12005.

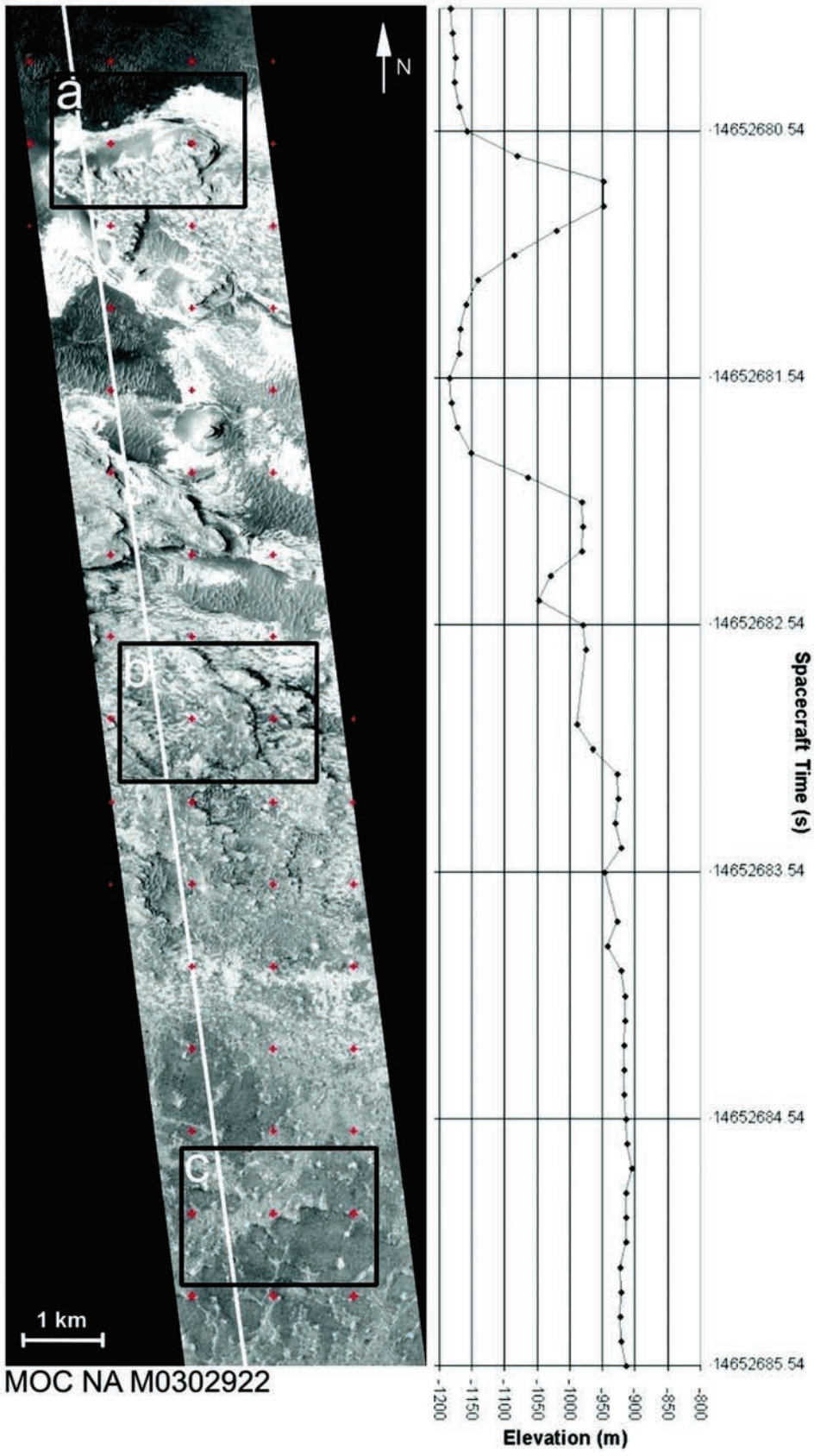

Figure 5a. MOC NA frame M03-02992 on eastern edge of Unit E showing transition from polygonal unit to buttes and mesas. Topographic profile shown from MOLA Orbit 11577 data, with elevations relative to the MOLA-defined datum. Note that the topography indicates that the polygonal unit is topographically and stratigraphically above the layered deposits that are exposed in the buttes and mesas.

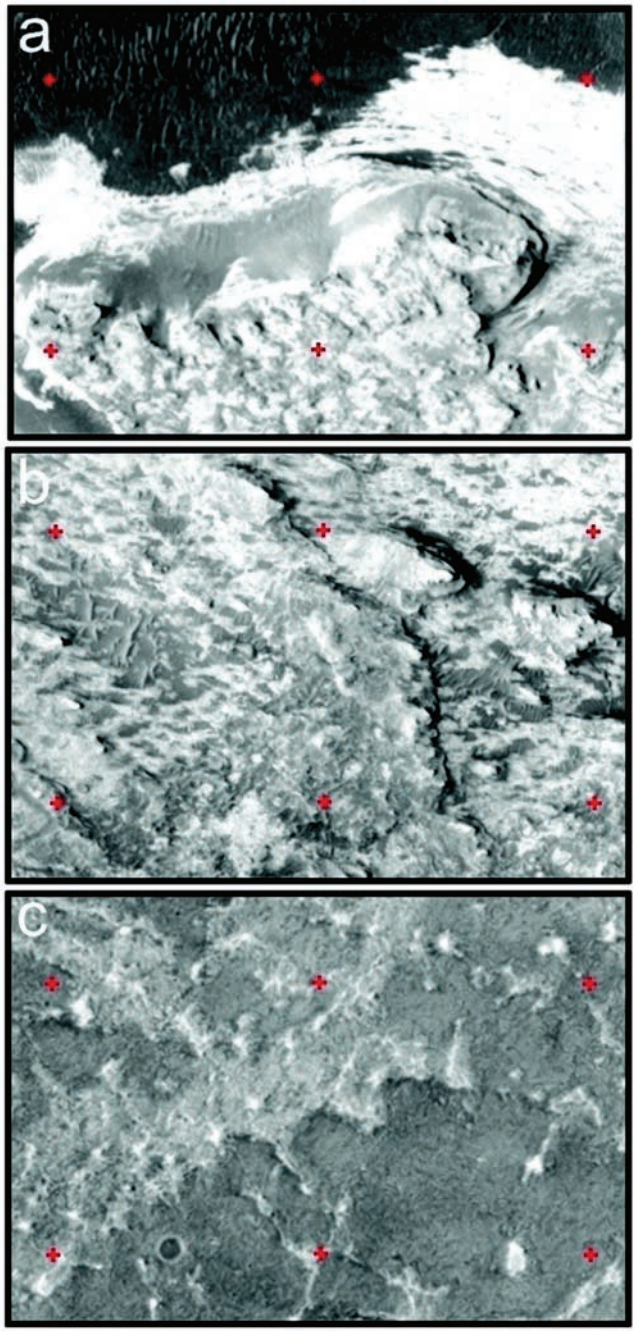

Figure 5b. Close-up views of portions of the NA frame showing details of the polygonal ground and the transition to the buttes and mesas. Note the strong zonal wind erosion and transport patterns. Unit DCT is exposed in the northern most portion of the subframe labeled "a".

ridges are exposed (Figures 4 and 8). We estimate a mantle depth of approximately 10 m near the boundary, thickening to the north.

3. Geologic Unit Albedo, Thermal Inertia, and Pulse Width Properties

[10] On a global basis there is a well-known negative correlation between albedo and thermal inertia, consistent with the dominance of: (a) bright, low thermal inertia dust-covered areas, (b) dark, high thermal inertia regions with exposed sands, and (c) an intermediate surface thought to contain weakly indurated materials, i.e., duricrust [*Mellon et al.*, 2001]. On a regional scale, the signature associated with Arabia Terra (north of study area, Figure 1) exhibits low thermal inertia and high albedo values indicative of dusty surfaces, whereas the dark region, Sinus Meridiani (northern portion is in study area), has low albedo and high thermal inertia values, and the Oxia Palus region (northwest of study area) has intermediate values falling into the zone interpreted to be due to duricrust exposures. With regard to the study site, Unit DCT falls within the globally defined low albedo, high thermal inertia cluster, whereas the Unit MCT falls within the duricrust cluster (Table 1 and Figure 9). Both plains units, P and Ph fall within the dark, high inertia cluster. On the other hand, Unit E has a distinctly high inertia and intermediate albedo that makes it stand out from the clusters defined on a global and even regional basis.

[11] In addition to its unusual combination of thermal inertia and albedo, Unit E is also distinct in that the unit boundaries mapped on the basis of topography and morphology also correspond well to the boundaries between relatively high and low thermal inertias areas (Figure 10). In addition, the TES-based bolometric albedo and MOLA-based pulse widths both show a high degree of spatial correlation with the distribution of Unit E, as does the spectral reflectance (0.4 to 1.0 micrometers) derived from Hubble Space Telescope data [*Morris et al.*, 2002]. In particular, the spectral data indicate that Unit E is bright and red relative to Ph and P, although not as bright as Unit MCT and areas to the north. The high degree of spatial correlation between mapped locations of Unit E and remote-sensing properties is unusual on Mars, given the extent to which aeolian activity has reworked the surface. We suggest that Unit E color, albedo, and thermal inertia are in fact representative of the mineralogy, texture, and degree of induration of materials that comprise this unit. In particular, results are consistent with an abundance of moderately consolidated materials that are bright and red as compared to dark areas on Mars.

[12] MOLA data can be used to infer terrain roughness by examining the extent to which the return pulse is broadened relative to the transmitted pulse [*Garvin et al.*, 1999]. In our case we have corrected the pulse spread for regional scale slopes, thus providing a measure of roughness at scales equal to or less than the MOLA footprint (150 m). Units P and Ph have the lowest MOLA corrected pulse width values, followed by Unit DCT (Figure 1 and Table 1), whereas the two remaining units, E and MCT, both have relatively high values. We offer two explanations for these trends. First, Unit MCT might retain a relatively rough topography associated with deposition and subsequent aeolian reworking of the accumulating materials. Second, Unit DCT may have been graded or beveled by aeolian erosion or volcanism and is thus smoother than the mantled areas. The rough signature associated with Unit E is interpreted to be due to differential aeolian erosion and consequent rough topography whereas the smooth signature associated with Units Ph and P are interpreted to be a consequence of deposition on an originally flat or rolling

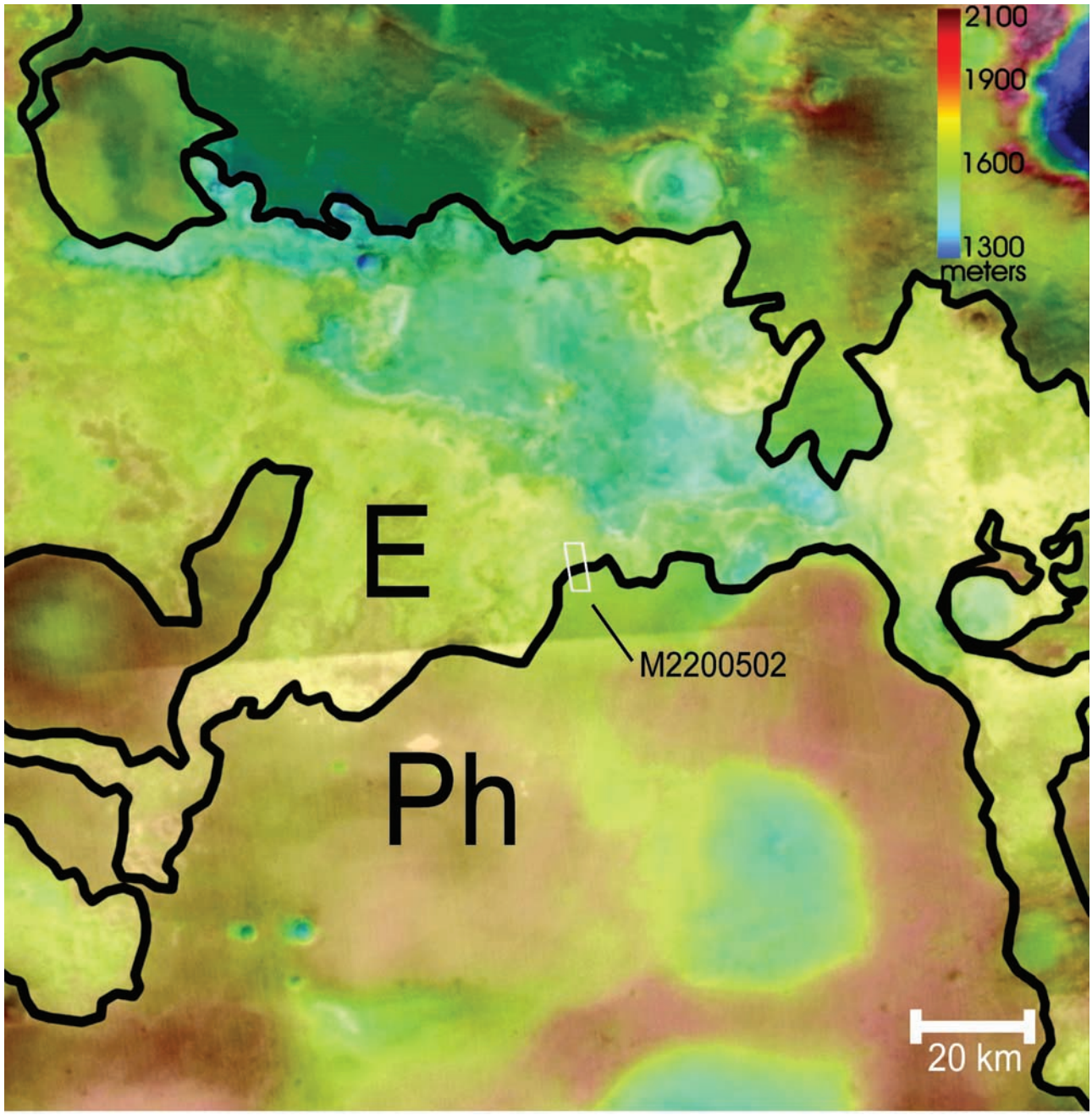

Figure 6a. MOC WA red frame mosaic overlain with color-coded elevations corrected for regional tilts showing northern boundary of hematite-bearing materials (Ph) and etched unit (E) outcrops located to the north as the topography slopes toward a NW-SE trending valley. Location of MOC NA frame shown.

surface that has been only locally reworked by aeolian processes.

4. Geologic Unit Spectral Emissivity Properties

[13] In this section we report on analyses of TES spectral radiance data for the four major mapped units in the study area. We note that with the exception of an abundance of hematite, Units Ph and P are indistinguishable and thus Unit P results will not be presented. The intent of our analysis was to evaluate the extent to which unit mineralogy can be inferred and used to understand the origin and evolution of the layered complex. As a first step in the analysis the TES spectral database provided through NASA's Planetary Data System was searched to find single-scan, dayside, low atmospheric opacity (optical depth less than 0.2), nadir observations without significant microphonic or other noise components. A total of 127,035 individual spectra passed the constraints and were extracted from the PDS archive. Each radiance observation was then converted to an apparent emissivity spectrum by dividing the observed radiance values by the values computed for a blackbody radiator with a kinetic temperature equal to the surface temperature reported in the TES standard product tables. Visual inspec-

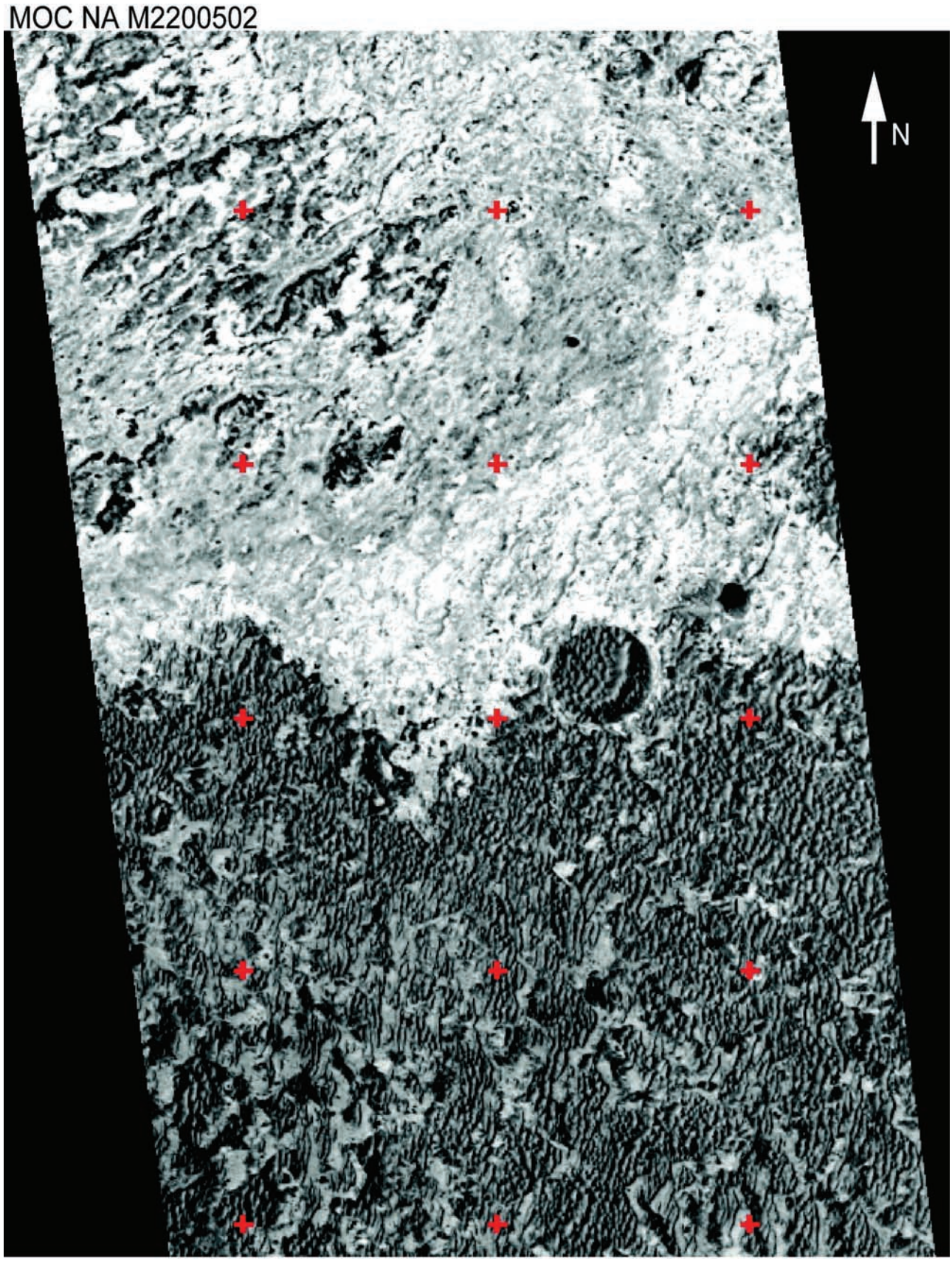

Figure 6b. MOC NA frame M22-00502 showing boundary between Units E and Ph. Unit E is exposed in the northern portion of the frame as the relatively bright materials with a strong morphologic grain running in a northeast to southwest direction. Ph consists of dunes superimposed on Unit E substrate. Note the strong easterly component inferred for dune transport.

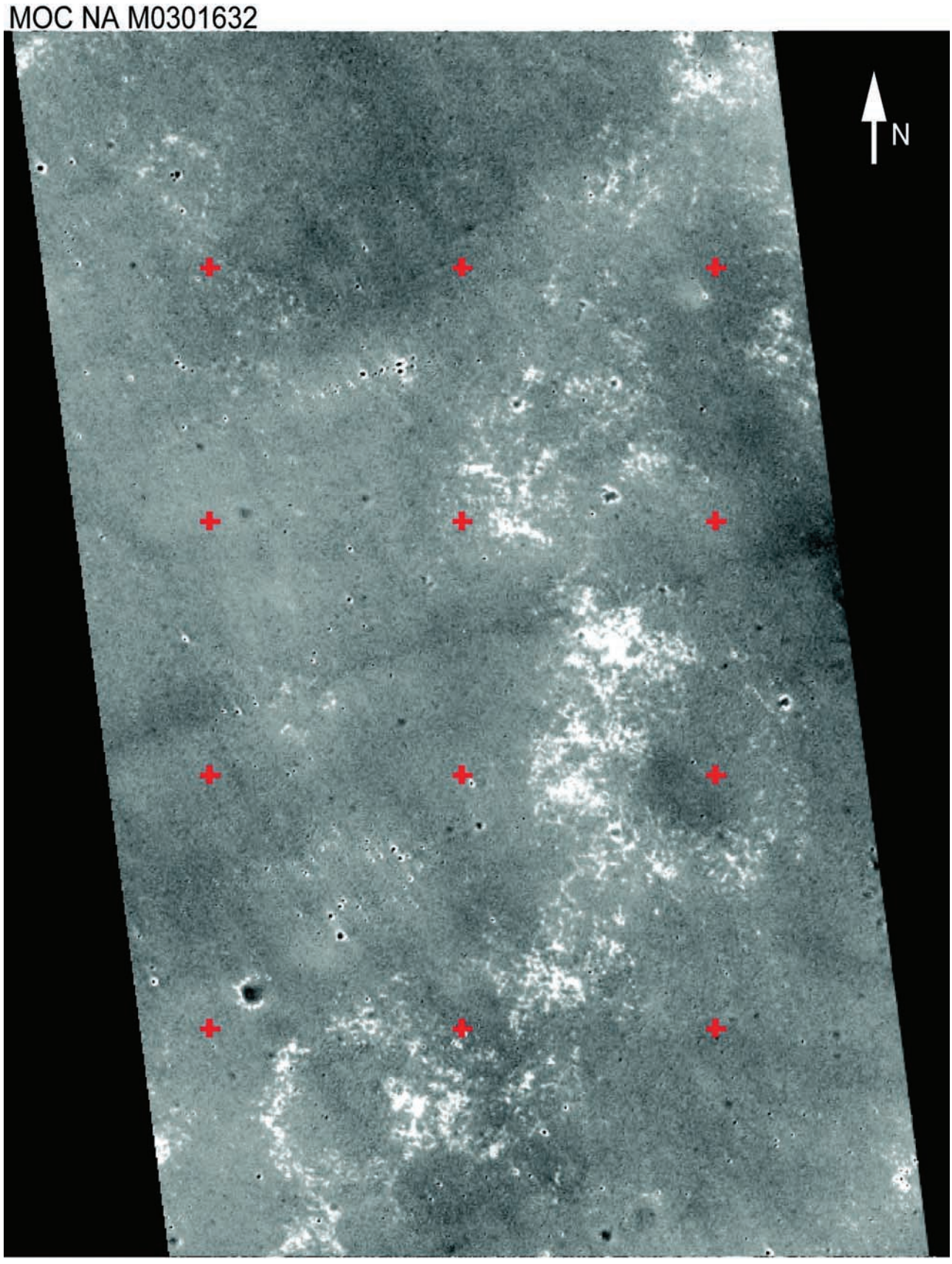

Figure 7. MOC NA frame M03-01632 within the MER landing error ellipse, showing dark surfaces and patches of brighter material. Small craters are also evident. The bright material is interpreted to be Unit E exposures.

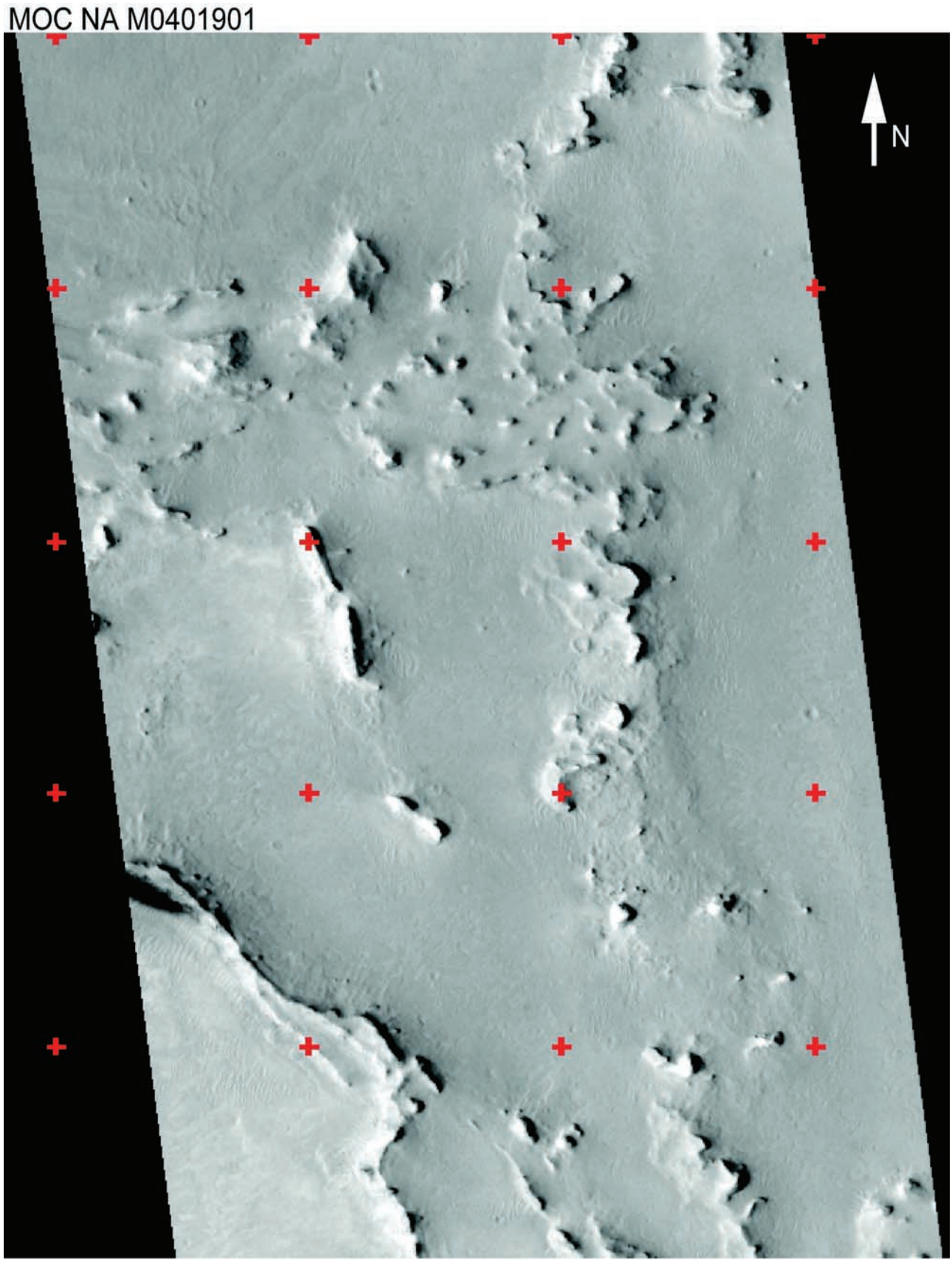

Figure 8. Mantled Unit E landforms are evident in this portion of MOC NA frame M04-01901. Linear ridges are 12 m above the plains based on analysis of MOLA data from MOLA Orbit 12005.

Table 1. Statistics for Units

Unit	Bolometric Albedo	Thermal Inertia, J/(m^2 K sqrt (s))	Corrected Pulse Width, m
MCT: Mantled Cratered Terrain	0.23 ± 0.01	227 ± 53	1.34 ± 0.83
Ph: Hematite Plains	0.15 ± 0.02	211 ± 27	0.68 ± 0.35
P: Plains	0.16 ± 0.02	232 ± 20	0.88 ± 0.60
E: Etched	0.19 ± 0.02	361 ± 77	1.35 ± 0.84
DCT: Dissected Cratered Terrain	0.15 ± 0.03	256 ± 40	0.81 ± 0.68

tion suggests that apparent emissivity spectra for Units Ph, E, and DCT are similar, although the Ph spectrum shows unique and strong evidence for hematite-related absorptions in the 300 to 500 cm^{-1} wave number region. On the other hand, the MCT spectrum has an overall higher apparent emissivity and a distinctly lower slope in the 800 to 1000 cm^{-1} spectral region as compared to the other spectra.

[14] The apparent emissivity spectral patterns are a combination of surface and atmospheric contributions. We have followed the method of *Smith et al.* [2000] in constructing a linear least squares unmixing approach for the separation of mean spectra for each mapped unit into atmospheric and surface spectral components (Appendix A). The surface spectra were recovered as a linear combination of 48 mineral end-members judged to be important components in prior surface mineralogy retrievals using TES data [e.g., *Bandfield et al.*, 2000; *Wyatt and McSween*, 2002]. The retrieved surface emissivity spectra confirm that Unit MCT is distinctly different in spectral properties as compared to the other three units (Figure 11). On the other hand, Units E, Ph, and DCT are very similar, except for the hematite-related absorptions in the Ph spectrum. These similarities have been quantified by computing the spectral angles between the various pairs of surface emissivity spectra. The spectral angle is related to the dot product of two spectra in channel space, such that an angle of zero radians indicates that the two spectra are identical and a large angle indicates significant variation from one spectrum to the other. The angle calculations demonstrate that Units DCT and E have the greatest affinity, followed by Units DCT and Ph (Table 2). Units MCT and Ph are the most dissimilar, followed by the MCT and DCT. These calculations provide quantitative verification of what can be

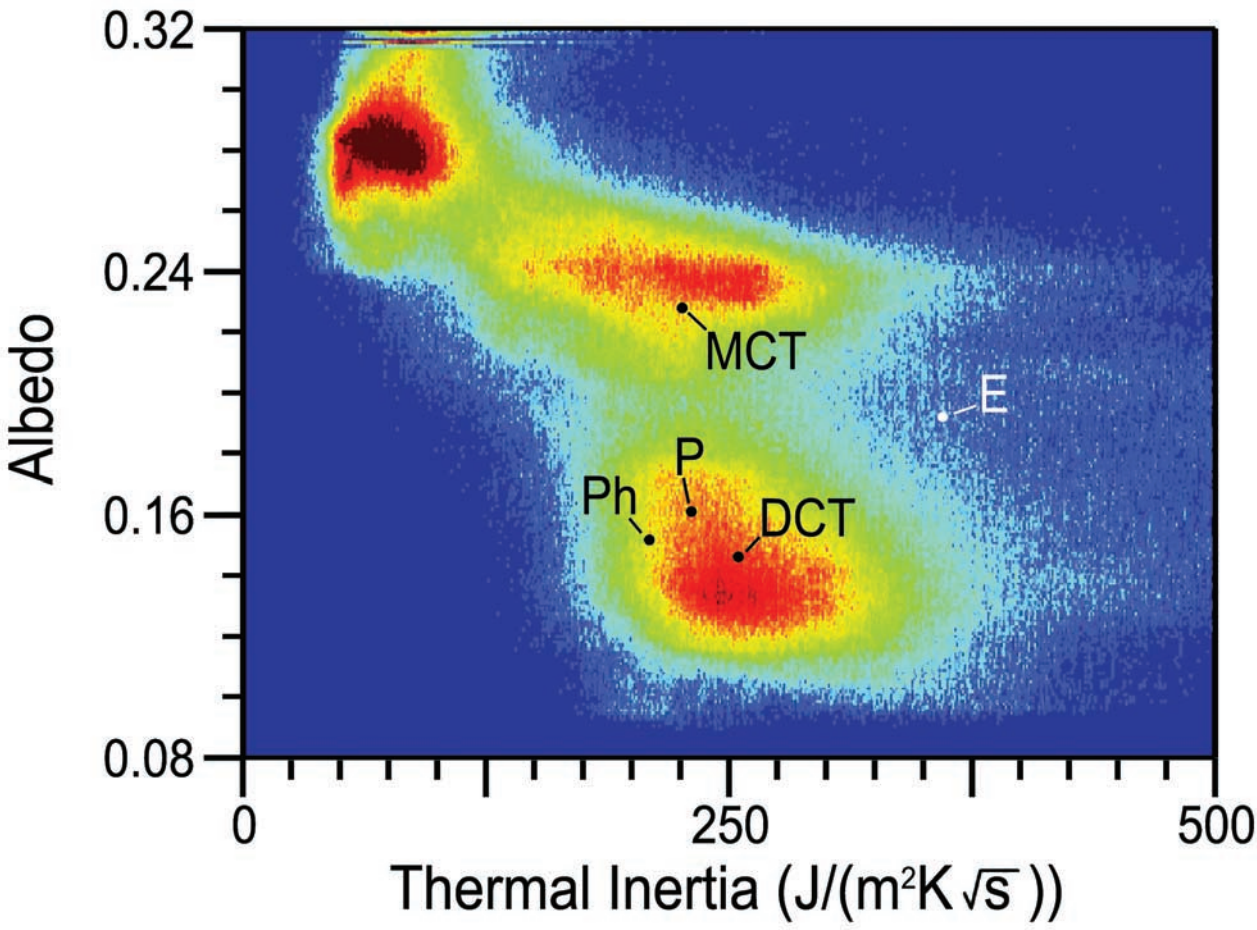

Figure 9. TES-based bolometric albedo vs. thermal inertia acquired for all longitudes and ±45° in latitude showing clusters interpreted to be bright dust (high albedo and low inertia), dark areas with coarser particles, and duricrust covered regions (intermediate albedoes and thermal inertias). Also shown are locations of mean values of albedo and thermal inertia for units mapped in Terra Meridiani study area.

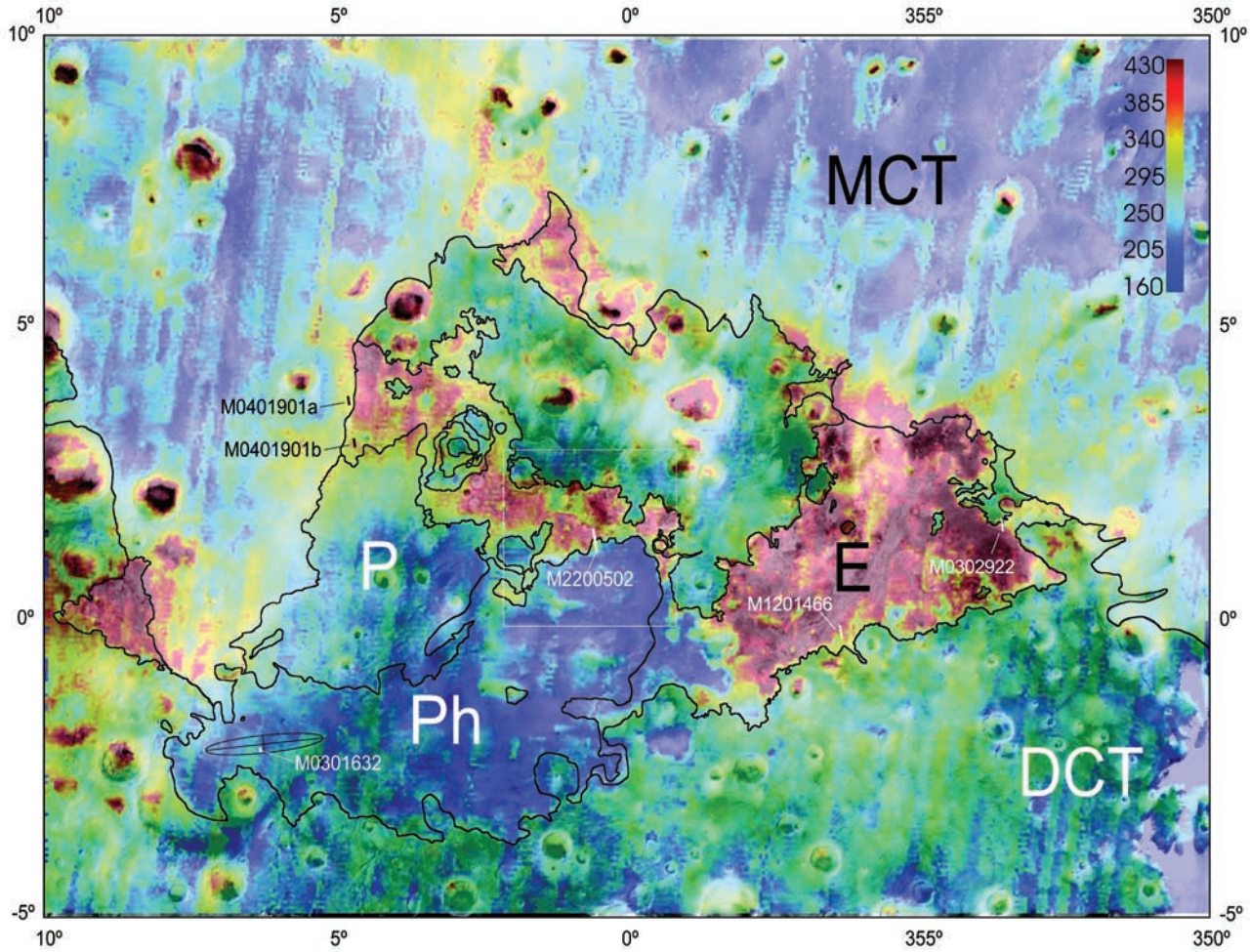

Figure 10. TES-based thermal inertia map with geologic unit boundaries overlain. Note the close correspondence between high thermal inertia and Unit E boundaries. The unit boundaries were mapped on the basis of morphology observed in MOC images, with the exception of the hematite index value used for the Ph boundary.

seen through examination of the apparent emissivity spectra and the retrieved surface spectra.

[15] The similarity of the derived surface spectra for Units DCT, E, and Ph indicates that these units are related mineralogically. To quantify this assertion we consider the minerals that are retrieved for the four units (Figure 12). Results show that retrievals for Units DCT and E are quite similar, dominated by plagioclase feldspar and clinopyroxene. The retrieval for Unit Ph is similar to those for Units DCT and E, but with a higher proportion of hematite. Unit MCT results are intriguing in that greater proportions of sulfates and phyllosilicates are indicated relative to the other three units. Further, there is a more equant distribution of plagioclase, microcline, and clinopyroxene.

[16] We note that linear unmixing of emissivity spectra is a powerful way to explore the data sets, but the method comes with provisos. First, it assumes that the emissivities of the end-members combine linearly. This assumption has been proven to be valid as long as the mineral grains are optically thick [*Feely and Christensen*, 1999]. This is probably the case for the Units DCT, Ph, and E, but may not be the case for the high albedo, low thermal inertia and thus presumably fine-grained Unit MCT materials. Second, the set of mineral spectra used as end-members must be representative of the material that comprise the unit and associated emissivity spectrum. This may or may not be the case for the Unit MCT, in particular, since the inferred induration and aeolian origin of this unit are consistent with a wider range of minerals than might be expected for the other units. Third, the end-members must be spectrally distinct in order to recover the proper mineral components and relative abundances. As shown by *Wyatt and McSween* [2002] the spectral coverage available for unmixing TES spectra leads to non-unique retrieval of volcanic glasses as opposed to phyllosilicates. Because of these issues we rank our interpretations in decreasing confidence as follows. Units DCT, E, and Ph are composed of similar materials, with the addition of hematite for Unit Ph. Unit MCT is mineralogically distinct from the other three units. Plagioclase and clinopyroxene dominate the Units DCT, E, and Ph. Each unit has some alteration products, including what appear to be sulfates and phyllosilicates. Phyllosilicates are

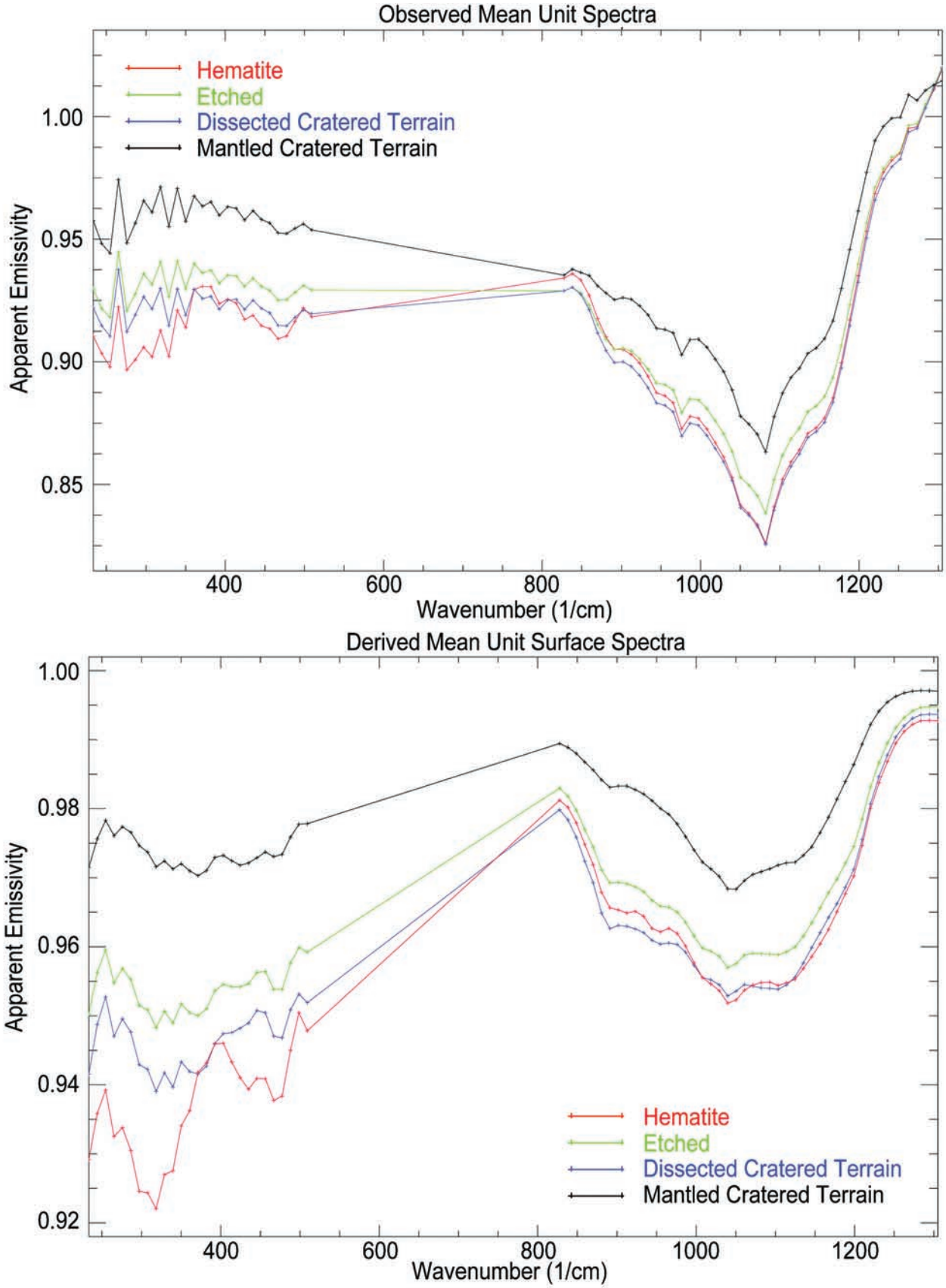

Figure 11. Plots of TES-based apparent spectral emissivity and retrieved surface spectra averaged for each of the four major units in the study area. Hematite corresponds to the Ph Unit.

Table 2. Spectral Similarity Angles[a]

–	DCT	E	Ph	MCT
DCT	0.0	0.17	0.37	0.54
E	0.17	0.0	0.50	0.38
Ph	0.37	0.50	0.0	0.84
MCT	0.54	0.38	0.84	0.0

[a]In degrees. Unit P is not shown.

predicted to be a dominate phase for MCT, consistent with the fine-grained nature of these deposits.

5. Hypothesis Development and Testing

[17] We consider in this section plausible explanations for emplacement of the layered complex (i.e., Units E, P, and Ph) and its unusual remote-sensing properties (Figure 13). To begin with, the morphologic and topographic evidence demonstrates that the layered complex was emplaced disconformably onto Unit DCT. Further, Unit E lies beneath P and Ph. At least the northern portion of the complex was covered by a widespread aeolian mantle that was cemented to become duricrust and most recently has been eroded by wind. The complex proper has also been exposed and differentially eroded by aeolian activity, providing a window into the stratigraphy of the units.

[18] The morphology of Unit E is complex and probably represents a combination of landforms associated with emplacement, burial, and differential aeolian erosion. We prefer a volcaniclastic origin for Unit E, and the entire complex, for several reasons. First, the deposits are widespread and not confined to a basin as they would be if the material accumulated in a lake or shallow sea. Second, the inferred mineralogy for the complex is dominated by igneous components, with the exception of hematite for the capping unit, Ph. Minerals such as pyroxene and feldspar would not survive well in a lacustrine or marine environment. Third, we interpret the regions within Unit E that expose dark polygons separated by bright ridges as exposing resistant materials that retain morphologic evidence for emplacement even after burial and exhumation (e.g., Figure 3). Specifically, we suggest the following scenario for the formation and evolution of these landforms. Lava flows were deposited onto Unit DCT and subjected to isotropic extension that fractured the flows into polygons. The pattern is remarkably similar to the portions of the fractured plains on Venus, both in terms of polygon widths and fracture patterns [*Johnson and Sandwell*, 1992]. Fracturing was followed by emplacement of dikes and flows that were in turn extended to form horst-graben patterns aligned with dike emplacement azimuths. These landforms were

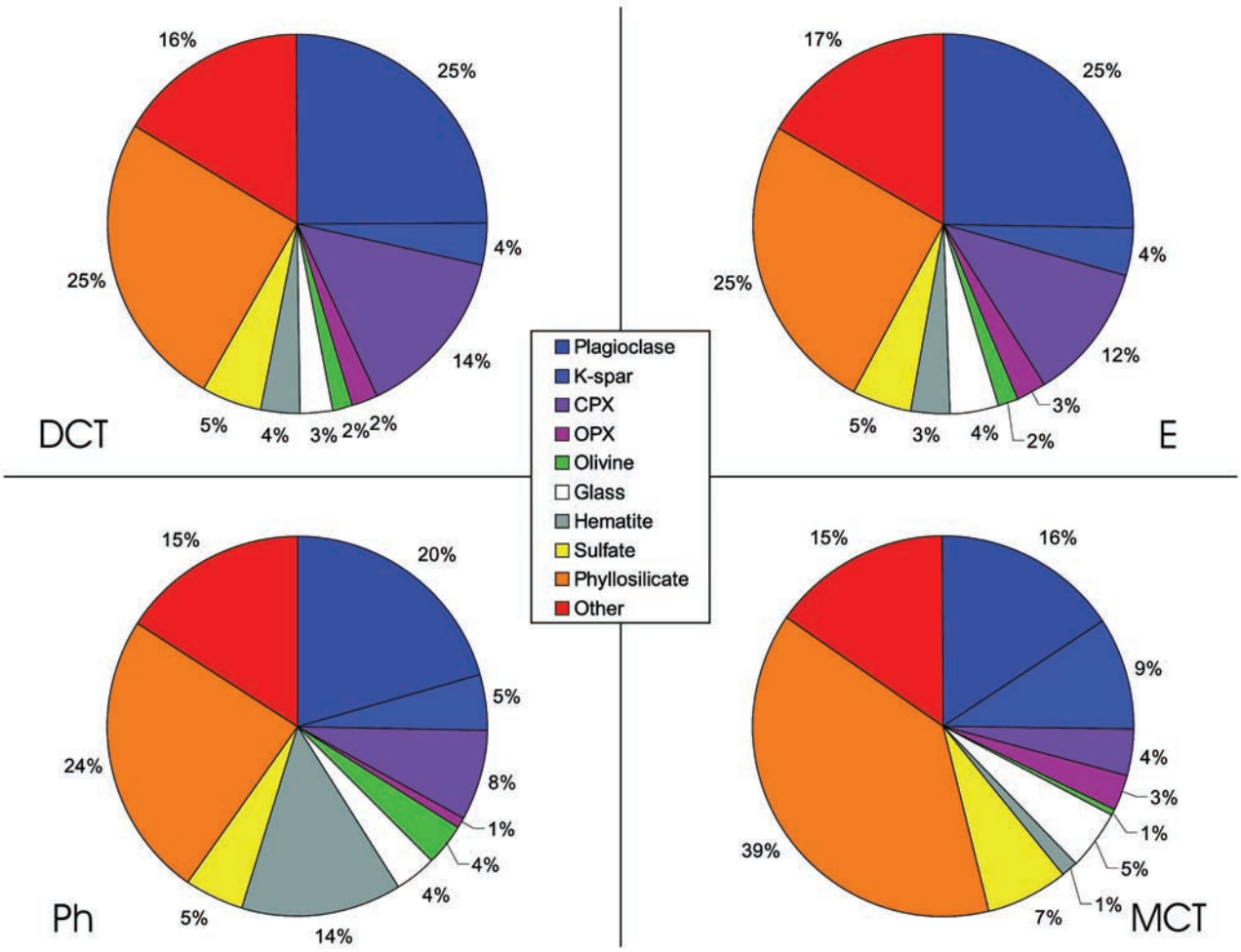

Figure 12. Pie charts showing the mineral proportions inferred from linear unmixing of average TES spectra for each unit in the study area.

Time Ordered History
Formation of Tharsis and associated load, causing lithosphere to tilt to the NW, with subsequent channel incision striking NW-SE
Emplacement of lava flows and tephra deposits disconformably onto dissected cratered terrain during extensional tectonic regime
Emplacement of hematite-bearing tephra deposits as last eruptive stage
Burial by regional-scale aeolian mantle
Aeolian exhumation of the mantle and underlying deposits, forming etched terrain and hematite-rich lag dunes

Figure 13. Summary of geologic history of Terra Meridiani study area.

then buried by volcaniclastic deposits and subsequently exhumed by wind (Figure 14). In other regions within Unit E the fractures became conduits for eruption of volcaniclastic materials (Figure 14). Widespread tephra blanketed these areas, followed by aeolian erosion to expose the deposits. Regions above the source dikes would have accumulated the thickest deposits and perhaps become the most indurated, thereby leaving behind ridges and stepped plateaus as the region was exhumed by wind (Figure 4). Units Ph and P are interpreted to represent the last stage of the volcaniclastic activity, producing what must have been a widespread cap that covered the complex. The hematite

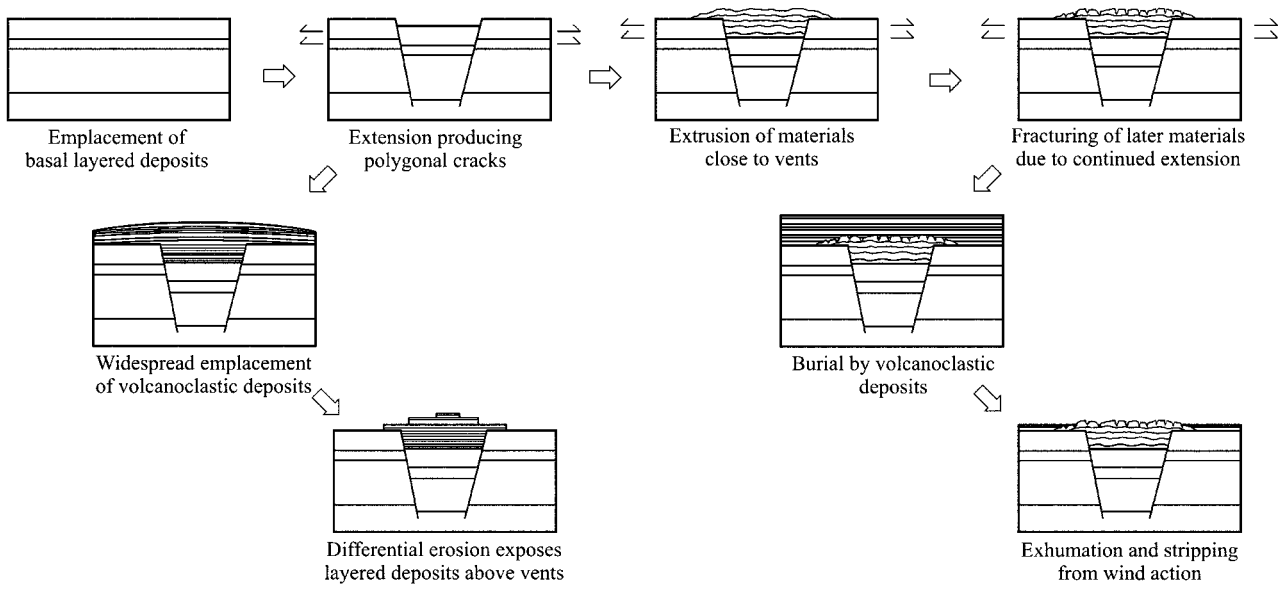

Figure 14. Schematic illustrations of the formation of extensional fractures tapping a magma source, emplacement of flows and tephra deposits, burial, and subsequent exhumation to explain the polygonal ground associated with Unit E.

Table 3. Athena Payload and Testable Hypotheses

Instrument	Key Parameters	Hypotheses to Test
	Mast-Mounted	
Pancam: Panoramic Camera	Twelve bands (0.4 to 1.0 μm) for multispectral, stereoscopic imaging with 0.3 mrad IFOV; 9.2 deg by 18.4 deg FOV.	*Mafic dunes with hematite-bearing grains sitting on brighter substrate? *Discrete hematite grains or found as glassy coatings? *Substrate shows evidence for volcanic emplacement, including eroded flows and tephra deposits?
Mini-TES: Thermal Emission Spectrometer	Emission spectra (5 to 29 μm, 10 cm^{-1} resolution with 8 or 20 mrad FOV)	*Substrate reflectance and emissivity are comparable to values for exposures of etched unit? Lithologic inferences?
	Arm-Mounted In Situ Package	
APXS: Alpha Particle X-Ray Spectrometer	^{244}Cm alpha particle sources, and x-ray detectors, 4 cm FOV	*Measurements on same samples before and after abrading rock surfaces confirm presence of glassy coatings produced during hydrothermal alteration?
MB: Mössbauer Spectrometer	^{57}Fe spectrometer in backscatter mode; Co/Rh source and Si-PIN diode detectors; field of view approximately 1.5 cm^2.	*Composition and mineralogy consistent with sedimentary or volcanic origin of deposits? If igneous, extent of differentiation?
MI: Microscopic Imager	30 μm/pixel monochromatic imager (1024 × 1024) with 6mm depth of field	*Rock and grain textures consistent with formation as flows and tephra deposits, reworked by aeolian activity?
RAT: Rock Abrasion Tool	Tool capable of preparing 5 mm deep by 4.5 cm wide surface on rocks	

bearing material within Ph has been locally reworked into dunes, probably as lag materials due to the high density of this mineral. In fact, the reworking would serve to disperse the material across the plains and disguise any evidence of source vents. This may help explain the unusual occurrence of hematite, pyroxene, and olivine, i.e., mechanical mixtures of an alteration phase and primary igenous minerals.

[19] A major remaining issue to be addressed is the explanation for the unusual remote-sensing properties associated with Units Ph and E. Unit Ph is dominated by igneous minerals and has a relatively high abundance of hematite. Hematite in this unit has been hypothesized to be present as gray, crystalline hematite grains formed in an aqueous environment [*Christensen et al.*, 2000b, 2001a], platy outcrops of hematite produced via metamorphism in the presence of water while the deposits were buried [*Lane et al.*, 2002], volcanic glass with embedded hematite crystals produced during high temperature devitrification [*Minitti et al.*, 2002], and as a primary igneous mineral produced during volcanic activity [*Noreen et al.*, 2001]. Our analyses suggest that the hematite is carried in the dark plains and dune forming materials, implying that the material is not exposed as platy outcrops. Our work does not shed light on whether the material exists as discrete grains or is contained within devitrified glass. Nor can we distinguish whether or not the hematite was produced as a primary volcanic product or via interactions with aqueous fluids.

[20] In the visible and reflected infrared wavelengths Unit E is brighter and redder than Unit Ph, although the spectral emissivity signature of Unit E is similar to dark regions (i.e., Unit DCT) and to the signature of Ph (sans hematite) and consistent with dominance by igneous minerals. We hypothesize that the unusual spectral characteristics associated with Unit E are due to glassy coatings that have been devitrified to cryptocrystalline clays with embedded nanocrystalline hematite crystals, i.e., similar to relatively bright, red (in visible and reflected infrared wavelengths) palagonite coatings found on Mauna Kea, Hawaii [*Morris et al.*, 2000]. In the thermal wavelengths the small crystals would show minimal or no distinctive signatures since the Reststrahlen bands would be minimized because of the interference of Fresnel and volume-dominated emission. We note that palagonite on Earth forms in the presence of water and associated oxidizing conditions, although it appears as if the temperature of formation and length of time to form this cryptocrystalline material is poorly constrained [*Schiffman et al.*, 2000].

[21] It is attractive to ascribe both the formation of the hematite in Unit Ph and the bright, red color of Unit E to the presence of devitrified glasses, although such an explanation is certainly non-unique. We are in a fortunate position to be able to test and update the hypotheses presented in this paper with the Athena Payload on the Mars Exploration Rover Mission (Table 3). The Opportunity Rover, while exploring the Ph unit, will be able to sample both the dark dune material (presumably the source of the hematite signature) and the brighter, underlying substrate that is hypothesized to be exposures of the underlying Unit E. The reason is that our examination of all NA frames within the landing error ellipse shows that this substrate is exposed in most places as patches of bright regions and subdued rolling plains and crater rims (Figures 2a, 2b, and 7). We hypothesize that that rover will find, over its expected traverse distances of hundreds of meters, exposures of the relatively bright substrate (i.e., Unit E) that underlies the hematite unit and the dark dunes and dark plains that contain hematite (i.e., Unit Ph).

[22] We expect that the mast-based remote-sensing package containing Pancam imaging and the Mini-TES emission spectrometer on the rover will be able to map the morphology, physical properties, and mineralogy of the sites visited. For example, questions that will be addressed include whether or not the hematite-bearing material appears within dunes as gray hematite grains or as glassy coatings. Or does the hematite occur as platy outcrops? Does the bright substrate show evidence for bright, glassy coatings in Pancam data and a mafic composition in spectral emissivity extracted from Mini-TES data? Further, the use of the Rock Abrasion Tool, coupled with the Microscopic Imager, Alpha Particle X-Ray and Mössbauer Spectrometers, will provide definitive tests of the hypotheses that the hematite exists as

*Mineral End-members**

Non-Silicates

Oxides	Hematite BUR-2600 Ilmenite WAR-4119 Magnetite WAR-0384
Carbonates	Calcite C27 Dolomite C28 Magnesite C55 Siderite C62
Sulfates	Anhydrite ML-S9 Gypsum ML-S6
Phosphates	Apatite ML-P1

Silicates

Olivine	FayaliteWAR-RGFAY01 ForsteriteAZ-01
OPX	BronziteNMNH-93527 EnstatiteHS-9.4B 51
CPX	AugiteNMNH-122302 AugiteNMNH-9780 DiopsideWAR-6474 Hedenbergite DSM-HED01
Amphibole	ActinoliteHS-116.4B Ferrohornblende HS-326.4B Hornblende NMNH-R7208 Magnesiohastingsite HS-115.4B Magnesiohornblende HS-315.4B
Serpentine	Serpentine BUR-1690 Serpentine HS-8.4B Antigorite NMNH-47108
Chlorite	Chlorite WAR-1924
Clays	Ca-montmorillonite STx-1g Fe-smectite SWa-1g Halloysite WAR-5102g Illite IMt-2g Kaolinite KGa-1bg Na-montmorillonite SWy-2g Nontronite WAR-5108g Saponite ASU-SAP01g
Micas	Biotite BUR-840 Muscovite WAR-5474
SiO2	Quartz BUR-4120
K-spar	Microcline BUR-3460 Anorthoclase WAR-0579
Plagioclase	Albite WAR-0244 Andesine BUR-240 Anorthite BUR-340 Bytownite WAR-1384 Labradorite WAR-4524 Oligoclase BUR-060D
Glass	Si Glass‡ SiKGlass MW-SiK-GLASS

Atmospheric End-members§

Dust	Dust Low CO_2 Dust High CO_2
Ice Clouds	Water Ice Cloud (Large Particles) Water Ice Cloud (Small Particles)
Isotope	CO_2 H_2O

Numerical End-members

Blackbody

*All minerals with a sample designation are from the ASU spectral library. See *Christensen et. al*, 2000b.

‡Provided by V. E. Hamilton.

§Provided by J. L. Bandfield.

Figure A1. Surface and atmospheric end-members.

discrete grains or glassy coatings on grains within the dunes and that material comprising the bright substrate is covered with palagonite-like coatings. All of the data will be used to test the idea that the materials and landforms were emplaced volcanically as flows and tephra deposits, mantled, and then exhumed by wind action. Finally, we expect that the complete data set will provide definitive tests of the nature and extent of interaction of the emplaced materials with aqueous fluids and thus dramatically increase our knowledge about the evidence for habitability and life on Mars.

Appendix A

[23] The linear unmixing procedure for TES spectra was performed with an end-member set consisting of six atmospheric spectra provided by J. L. Bandfield (personal communication, 2002), a blackbody spectrum to account for variations in spectral contrast, and 48 pure mineral spectra (Figure A1). The primary output of the unmixing procedure is the unity-normalized parameter set assigned to the mineral end-members. These values correspond to the fractional areal coverage of each end-member within the field of view of the instrument at the time of observation. The mean normalized value for each end-member within each of the four main surface units was calculated, and the mineral end-members were grouped into the mineral classes shown in Figure 12.

[24] **Acknowledgments.** REA and FPS were supported by the NASA Planetary Geology and Geophysics Program through Grant NAG5-7830 from the Goddard Space Flight Center and by the Mars Exploration Rover Mission under contract from Cornell University. We thank the NASA Planetary Data System for access to the MGS archives used in our analyses. We also thank Philip Christensen, Joshua Bandfield, Vicky Hamilton, and Steven Ruff, Arizona State University, for help in understanding their approach to analysis of TES data.

References

Bandfield, J. L., V. E. Hamilton, and P. R. Christensen, A global view of Martian surface compositions from MGS-TES, *Science*, *287*, 1626–1630, 2000.

Caplinger, M. A., and M. C. Malin, Mars Orbiter Camera geodesy campaign, *J. Geophys. Res.*, *106*, 23,595–23,606, 2001.

Christensen, P. R., et al., Detection of crystalline hematite mineralization on Mars by the Thermal Emission Spectrometer: Evidence for near-surface water, *J. Geophys. Res.*, *105*, 9623–9642, 2000a.

Christensen, P. R., et al., A thermal emission spectral library of rock-forming minerals, *J. Geophys. Res.*, *105*, 9735–9739, 2000b.

Christensen, P. R., et al., Mars Global Surveyor Thermal Emission Spectrometer experiment: Investigation description and surface science results, *J. Geophys. Res.*, *106*, 23,823–23,871, 2001a.

Christensen, P. R., R. V. Morris, M. D. Lane, J. L. Bandfield, and M. C. Malin, Global mapping of Martian hematite deposits: Remnants of water-driven processes on early Mars, *J. Geophys. Res.*, *106*, 23,873–23,886, 2001b.

Feely, K. C., and P. R. Christensen, Quantitative compositional analysis using thermal emission spectroscopy: Application to igneous and metamorphic rocks, *J. Geophys. Res.*, *104*, 24,195–24,210, 1999.

Garvin, J. B., J. J. Frawley, and J. B. Abshire, Vertical roughness of Mars from the Mars Orbiter Laser Altimeter, *Geophys. Res. Lett.*, *26*, 381–384, 1999.

Hynek, B. M., and R. J. Phillips, Evidence for extensive denudation of the Martian highlands, *Geology*, *29*, 407–410, 2001.

Hynek, B. M., R. E. Arvidson, and R. J. Phillips, Geologic setting and origin of Terra Meridiani hematite deposit on Mars, *J. Geophys. Res.*, *107*(E10), 5088, doi:10.1029/2002JE001891, 2002.

Johnson, C. L., and D. T. Sandwell, Joints in Venusian lava flows, *J. Geophys. Res.*, *97*, 13,601–13,610, 1992.

Lane, M. D., R. V. Morris, S. A. Mertzman, and P. R. Christensen, Evidence for platy hematite grains in Sinus Meridiani, Mars, *J. Geophys. Res.*, *107*(E12), 5126, doi:10.1029/2001JE001832, 2002.

Malin, M. C., and K. S. Edgett, Mars Global Surveyor Mars Orbiter Camera: Interplanetary cruise through primary mission, *J. Geophys. Res.*, *106*, 23,429–23,570, 2001.

Mellon, M. T., B. M. Jakosky, H. H. Kieffer, and P. R. Christensen, High-resolution thermal inertia mapping from the Mars Global Surveyor Thermal Emission Spectrometer, *Icarus*, *148*, 255–437, 2001.

Minitti, M. E., M. D. Lane, and J. L. Bishop, Oxidized volcanic materials as a potential explanation for the gray hematite region on Mars, *Lunar Planet. Sci.*, *XXXII*, 1674, 2002.

Morris, R. V., et al., Mineralogy, composition, and alteration of Mars Pathfinder rocks and soils: Evidence from multispectral, elemental, and magnetic data on terrestrial analogue, SNC meteorite, and Pathfinder samples, *J. Geophys. Res.*, *105*, 1757–1817, 2000.

Morris, R. V., J. F. Bell III, W. H. Farrand, and M. J. Wolff, Constraints on Martian global surface mineralogic composition, albedo, and thermal inertia from Hubble Space Telescope extended visible multispectral data, *Lunar Planet. Sci.*, *XXXII*, abstract 1913, 2002.

Noreen, E., K. L. Tanaka, and M. G. Chapman, TES hematite landing sites in Sinus Meridiani for 2003 Mars Exploration Rover, paper presented at 2003 MER Landing Site Workshop, Lunar and Planet. Inst., Pasadena, Calif., 2001.

Phillips, R. J., et al., Ancient geodynamics and global-scale hydrology of Mars, *Science*, *291*, 2587–2591, 2001.

Schiffman, P., et al., Controls on palagonitization versus pedogenic weathering of basaltic tephra: Evidence from the consolidation and geochemistry of the Keanoakako'i Tephra Member, Kilauea Volcano, *Geochem. Geophys. Geosyst.*, *1*, Paper number 2000GC000068, 2000.

Smith, D. E., et al., Mars Orbiter Laser Altimeter: Experiment summary after the first year of global mapping of Mars, *J. Geophys. Res.*, *106*, 23,689–23,722, 2001.

Smith, M. D., J. L. Bandfield, and P. R. Christensen, Separation of atmospheric and surface spectral features in Mars Global Surveyor Thermal Emission Spectrometer (TES) spectra, *J. Geophys. Res.*, *105*, 9589–9607, 2000.

Wyatt, M. B., and H. Y. McSween, Spectral evidence for weathered basalt as an alternative to andesite in the northern lowlands of Mars, *Science*, *417*, 263–266, 2002.

R. E. Arvidson, K. S. Deal, B. M. Hynek, J. M. Kieniewicz, W. C. Koeppen, F. P. Seelos IV, and N. O. Snider, McDonnell Center for the Space Sciences, Department of Earth and Planetary Sciences, Washington University, Campus Box 1169, One Brookings Drive, St. Louis, MO 63130, USA. (arvidson@wunder.wustl.edu)

J. B. Garvin, NASA Goddard Space Flight Center, Greenbelt, MD 20771, USA.

M. T. Mellon, Laboratory for Atmospheric and Space Physics, University of Colorado, Duane Physics Building, Campus Box 392, Boulder, CO 80309-0392, USA.